Study on the dynamics of chitosan/cotton fiber in an airflow around two rotating cylinders

Hui Fen Guo[1], Chenxiao Yang[1] and Li Li[2*]

[1]*The Hong Kong Polytechnic University QT702, The Hong Kong Polytechnic University, Kowloon, Hong Kong*

[2]*The Hong Kong Polytechnic University QT702, The Institute of Textiles and Clothing, The Hong Kong Polytechnic University, Kowloon, Hong Kong*

*Corresponding author:

Li Li, The Hong Kong Polytechnic University QT702, The Institute of Textiles and Clothing, The Hong Kong Polytechnic University, Hunghom, Kowloon, Hong Kong.
Email: li.lilly@polyu.edu.hk

Abstract

To predict chitosan/cotton yarn properties in ring spinning, a particle-level simulation method has been used to simulate the dynamics of the fibers with different initial positions in three-dimensional airflow around counter-rotating cylinders. The results show that the fibers near the cylinder end-face can leave two cylinders' nip and move around the top cylinder, thus form fly waste. It is good to entangle other fibers as this gives the fiber greater bending energy. Compared with cotton fiber, the axial-direction deflections of the tail-ends of chitosan fibers near the cylinder center are much greater, while their bending energies are much lower, thus forming a wide triangle zone and reduced fiber–fiber cohesion force and yarn strength. To demonstrate the simulation results, a series of spinning experiments are completed, which tally with the predictions.

Keywords

chitosan, cotton, fiber dynamics, spinning triangle, rotating flow

Introduction

Chitosan (CS) is an excellent biomaterial, and has drawn much attention in research and industry because it is nontoxic, edible, biocompatible, biodegradable, bacteriostatic, and fungistatic.[1] All these features make CS a promising material for widespread applications. For example, in the area of textiles, CS can be used to make functional materials and fabrics, and also for textile wet processing, including dyeing, printing, durable press, antistatic finishes, etc.[2] However, the use of CS is limited due to its poor mechanical properties, weak barrier properties of the film, and high moisture sensitivity.[3] Moreover, the production cost of CS fiber is higher than that of others. Blending of different fibers in the textile industry is an alternative way to use the good properties of the components and incorporate the more desirable features of the constituent fibers. The CS–cotton blend yarn could be an ideal method to balance cost and functionality. At present, most of the information available in the literature on CS–cotton yarn properties is based on spinning experiments,[4] but a combined theoretical and numerical study of this subject is rarely reported in the published literature.

Due to both low strength and poor spinnability of CS, ring spinning, which contributes to higher yarn quality and is more flexible in application compared to other spinning systems, is used to produce CS–cotton blended yarn.[4] In the ring-spinning process, the drafted fiber strand leaves the front roller nip and is twisted into a yarn. This twist region between the front roller nip and the fiber convergence point is called the spinning triangle, which is a critical region. In this triangle zone, the fibers are transformed and transferred around other fibers and enhance friction between fibers, which is beneficial for yarn strength and wear resistance.[5] Obviously, the motion and interaction of the fibers in the triangle zone are closely related to their dynamics. Also, as the front roller pairs make an equal high-speed and reverse rotation, a rotating airflow is created. Due to the effects of the rotating flow, the flexible fibers are transferred and rotated around the neighboring fibers, resulting in the fibers twisting into the convergence point to form the triangle zone. Therefore, the dynamics of flexible fibers in rotating flows is of great interest to predict the product properties, and to optimize the design of the spinning systems. In this paper, we will set up a fiber model to study the dynamics of CS–cotton fibers in a rotating flow (the spinning triangle) and analyze the product properties using a numerical method.

It is known that the textile fibers have a large ratio of length to radius, i.e., aspect ratio, and at the same they are elastic and flexible. Therefore, the dynamics of flexible fibers are very complicated. The particle-level simulations, in which the fibers are represented by multiple rigid-body systems of hydro-dynamically simple particles, may be a useful complement to theoretical and experimental investigations. Yamamoto and Matsuoka[6] regarded a fiber as a group of spheres that are lined up and bonded to each neighbor (called a bead-chain). Each pair of bonded spheres can stretch, bend, and twist, by changing the bond distance, bond angle, and torsion angle. Ross and Klingenberg[7] represented a fiber as a series of rigid prolate spheroids connected end-to-end, whose model eliminated the need for iterative constraints to maintain fiber connectivity in the bead-chain[6] and represented large aspect ratio fibers with relatively few rigid bodies. It was further explored by Dong and colleagues[8] to account for fiber–wall interaction. A disadvantage of the approach of Ross and Klingenberg[7] is the difficulty of finding interfiber separations among spheroids. To overcome such restrictions, Schmid and colleagues modeled flexible fibers as chains of circular cylinders with hemispherical end-caps connected by ball-and-socket

joints.[9] Based on small deflection theory,[10] we have introduced a bead–rod-chain fiber model,[11,12] in which the rods only serve to transmit forces and maintain the configuration of the fiber, to calculate the motion of the flexible fiber in a swirling flow. This model can also save computational time because fewer beads are used.

In this study an extended 3D bead–rod-chain fiber model of Guo and Xu[11,12] is employed to simulate the dynamics of CS–cotton fibers in the 3D rotating flow in a spinning triangle. To simulate the motion of a flexible fiber in a flow field, the one-way coupling Euler–Lagrange approach is utilized. The flow field is first obtained by solving Navier–Stokes equations with dynamic meshes using the finite-volume approach, and then fiber dynamics are investigated by solving the bead–rod model equations describing the response of an elastic fiber to the combined forces exerted on it by the fluid flow. Finally, to verify numerical predictions, a set of corresponding spinning experiments is designed.

Computational method

Numerical simulation of fluid flow

In spinning studies, the drafting system is mostly inclined at an angle $\theta = 45°$ with respect to the horizontal plane, and the front top rollers' central axes are displaced forward by 3 mm relative to the corresponding central axes of the bottom rollers.[5,13] For the convenience of modeling, the rollers are simplified as circular cylindrical shapes. Figure 1 shows the profile with two rotating cylinders used in a 3D simulation. The origin of the 3D Cartesian coordinate system is located at the center of the axis of the upper cylinder without the offset. The z-axis is along the axial direction of the cylinders and the y-axis is vertical, pointing downwards. The x–z plane is the horizontal plane and the x–y plane is parallel to the cross-sections of the cylinders. The computation constants are given as follows: The length of the two circular cylinders is 28 mm, and their diameters are 25 mm for the lower cylinder and 28 mm for the upper one. The distance between two cylinder centers is 0.3 mm. The rotational speed of the bottom roller (lower cylinder) of 240 rpm is used.

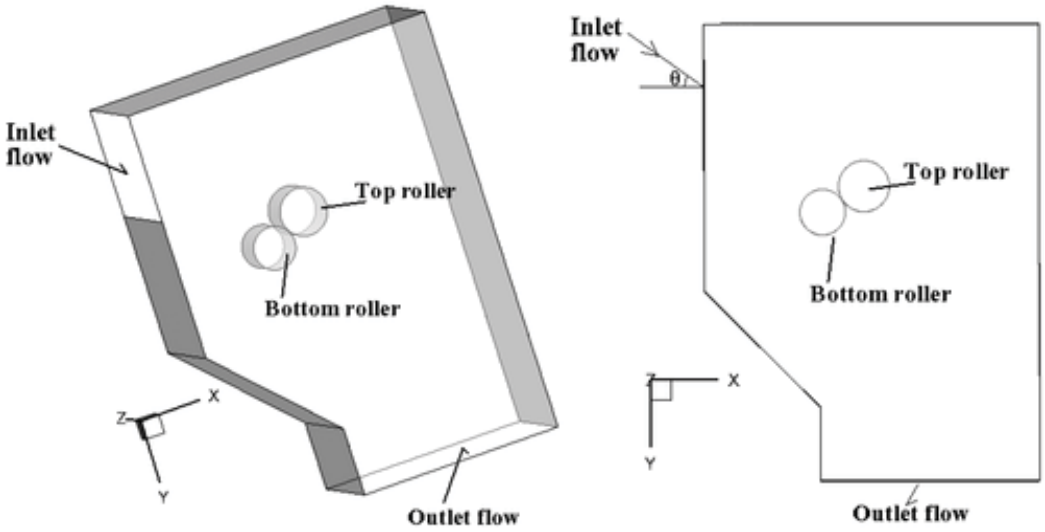

Figure 1. Profiles of the 3D model and *z*-direction projection for 45° inclination angle and the 3 mm forward offset of the top roller.

In this paper, the flow field can be considered to be viscous, unsteady, and incompressible flows; time-averaged conservation equations are used to calculate the flows. The governing equations are given as:

$$\nabla \cdot \mathbf{u} = 0 \frac{\partial \mathbf{u}}{\partial \mathrm{t}} + (\mathbf{u} \cdot \nabla)\mathbf{u} = -\nabla \mathrm{P} + Re^{-1} \nabla^2 \mathbf{u} \tag{1}$$

where $\mathbf{u} \equiv (u, v, w)$ is the velocity field, t is the time, P is the static pressure, and Re is the Reynolds number.

To perform numerical simulations around two rotating circular cylinders, the dynamic mesh technology is adopted.[14,15] With respect to dynamic meshes, on an arbitrary control volume, V, the integral form of the conservation equation for a general flux, φ, is written as:

$$\frac{d}{\mathrm{dt}} \int_V \rho \varphi \mathrm{d}V + \int_{\partial V} \rho \varphi (u - u_g) \cdot \frac{\mathrm{d}}{A} = \int_{\partial \mathrm{V}} \Gamma \nabla \varphi \cdot \mathrm{d}\vec{A} + \int_V S_\varphi \mathrm{d}V \tag{2}$$

where ρ is the air density, $\boldsymbol{u}_g$ is the mesh velocity of the moving mesh, Γ is the diffusion coefficient, and S_φ is the source term. ∂V is used to represent the boundary of the control volume.

In the present computation, the finite-volume code Fluent is used. The computational procedure is simplified by limiting the deformations to the two rotating cylinders' domain and grids, in which all the computational domains are set as stationary domains. The mesh updates are obtained through systematic implementations of spring-based smoothing[14]and local remeshing.[15]

Flexible fiber dynamics model

The dynamics of a flexible fiber in a fluid field depends on the fiber properties such as stiffness, fiber length, the surface roughness, and cross-sectional deformation. To simplify, the surface roughness and cross-sectional deformation of the fiber are ignored and a fiber with equal diameter and smooth surface is assumed. The fiber extensibility is important here since the fiber will be stretched in the textile drafting system. Therefore, we will extend the bead–rod fiber model of Guo and Xu by considering the stretching force of the fiber in this study.[11,12] The fiber is composed of n beads of radius r, which are connected by n – 1 mass-less rods. Only beads are affected by the stretching, bending, and twisting restoring forces, as well as the hydro forces from the fluid, and the rods only serve to transmit forces and maintain the configuration of the fiber. In this section, only a brief outline of the fiber model is described. A detailed description of the fiber model and the computational method are available from Guo and Xu.[11]

Based on small deflection theory,[10] the fiber stretch, bend, and twist can be described by changing the displacements of two, three, or four adjacent beads, respectively (Figure 2). The stretching $\boldsymbol{F}_i^s$, bending $\boldsymbol{F}_i^b$, and twisting $\boldsymbol{F}_i^t$ restoring forces exert on the bead i:

$$F_i^s = \frac{\pi r^2 E}{l_{i-1,i}} \Delta l e_{i-1,i} \quad F_i^b = -\frac{3\,\mathrm{El}_b}{l_{i-1,i}^3} \mathbf{s}_b \quad F_i^t = -\frac{\mathrm{GI}_t}{l_s l_{i-2,i-1}} \mathbf{s}_t \tag{3}$$

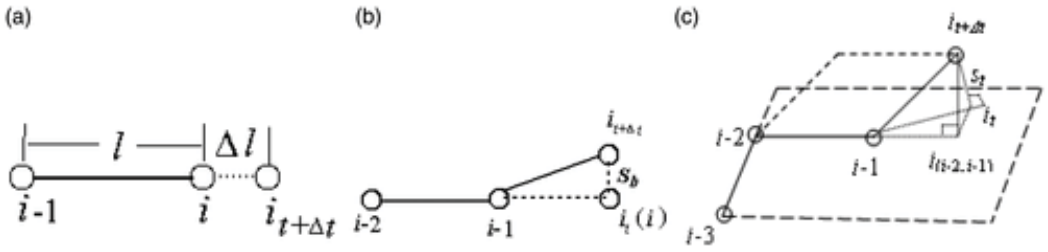

Figure 2. Sketch of the fiber deformations for (a) stretching; (b) bending; and (c) twisting.

As shown in Figure 2, Δl and $\boldsymbol{e}_{i-1,i}$ are the extension and unit vectors of the fiber section $(i-1, i)$, respectively; $(i-1, i_t)$ is the equilibrium position of the fiber section $(i-1, i)$; and the fiber section will be bent when the bead i moves from i_t to $i_{t+\Delta t}$. The fiber section $(i-1, i_{t+\Delta t})$ is the position after torsion of $(i-1, i)$ and the line $(i_{t+\Delta t}, i_t)$ is normal to the plane comprising the fiber sections $(i-2, i-1)$ and $(i-3, i-2)$. $\boldsymbol{s_b}$ is the bending deflection of the section $(i-1, i)$ and $\boldsymbol{s_t}$ is the twisting displacement of the section $(i-2, i-1)$. E and I_b are Young's modulus and the moment of inertia of the fiber cross-section area, respectively. G and I_t are the shear modulus and the polar moment of inertia, respectively. $l_{i-1,i}$ and $l_{i-2,i-1}$ are the fiber lengths from its adjacent beads $i-1(i-2)$ and $i(i-1)$, respectively. l_s is the length of the line segment $(i_{t+\Delta t}, i_{(i-2,i-1)})$.

In this paper, only drag force is considered. For the bead i, the drag force $\boldsymbol{F}_i^d$ is contributed by fiber sections $(i-1, i)$ and $(i, i+1)$. It can be calculated by:

$$F_i^d = (F_{i-1,i}^d + F_{i,i+1}^d)/2 \tag{4}$$

$\boldsymbol{F}^d_{i-1,i}$ and $\boldsymbol{F}^d_{i,i+1}$ are the drag forces acting on the bead i, which are devoted to the fiber sections $(i-1, i)$ and $(i, i+1)$, respectively. To obtain these forces, the method of equivalent volume is used when the fiber section is regarded as a cylindrical rod. Therefore, the drag $\boldsymbol{F}^d_{i-1,i}$ acting on the fiber section $(i-1, i)$ can be expressed as:

$$F_{i-1,i}^d = \pi d_v^2 C_D \rho \left|V_i - V_{\mathrm{fi}}\right|(V_i - V_{\mathrm{fi}})/8 \tag{5}$$

where $d_v = (6r^2 l_{i-1,i})^{1/3}$ is the equivalent diameter of an equal volume sphere. C_D is the drag coefficient. $\boldsymbol{V}_i$ and $\boldsymbol{V}_{fi}$ are the fluid and fiber velocities at the mass center of the fiber section ($i-1$, i), respectively.

In addition, since the gap between two cylinders (roller nip) is very small, the fiber will frequently touch two cylinder walls, thus, a simple particle-wall collision model is adopted here. In this paper, the dependence of the normal e_n and tangential e_t coefficients of restitution on the collision angle, α, was assumed to follow the relation obtained by Grant and Tabakoff:[16]

$$e_n = 0.993 - 1.76\alpha + 1.56\alpha^2 - 0.49\alpha^3 e_t = 0.988 - 1.66\alpha + 2.11\alpha^2 - 0.67\alpha^3 \quad (6)$$

According to Newton's second law, the equations of motion for the bead i that constitute the fiber are given as:

$$m_i d\mathbf{V}_{fi}/\mathrm{dt} = \mathbf{F}_i^s + \mathbf{F}_i^b + \mathbf{F}_i^t + \mathbf{F}_i^d \, d\mathbf{X}_i/\mathrm{dt} = \mathbf{V}_{fi} \quad (7)$$

where X_i and m_i are the displacement and mass of the bead i, respectively.

When solving the dynamic (7) of the fiber, due to numerical errors, the following connectivity of the fiber chain, i.e., the nonslip conditions, may be broken.

$$\sum(X_i - X_{i-1}) = l_f \quad (8)$$

where X_{i-1} and X_i are the position vectors of adjacent beads $i-1$ and i, respectively. l_f is the total length of the fiber. Similar to the method of Doi and Chen,[17] to remove this problem at each time step the positions of the beads are slightly adjusted from $\boldsymbol{X}_i$ to $\boldsymbol{X}_i + \Delta\boldsymbol{X}_i$ in such a way that the quantity of the function $\sum(\Delta\boldsymbol{X}_i)^2$ becomes minimum.

Experimental

For qualitative verification of numerical results of the fiber dynamics in the spinning triangle, 20 (Ne) yarn samples including pure cotton (CT), pure chitosan (CS), and the chitosan–cotton (CS–CT) blend with 50% cotton ratio were produced in the ring-spinning system using the same production conditions. Cotton and chitosan fibers were used as raw materials for the preparation of the samples. The raw material properties of the CS and CT fibers used in this study, which were measured by INSTRON 5566 according to ASTM standard D1577, are given in Table 1.

	Length (mm)	Fineness (Denier)	Tenacity (cN/tex)	Breaking extension (%)	Young's modulus (cN/tex)
Cotton (CT)	37	1.6	16.89	12.3	344.22
Chitosan (CS)	38	1.81	15.49	23.45	521.24

Table 1. Physical properties of cotton and chitosan fibers

All these yarns are tested on an automatic single-yarn strength tester with a testing speed of 200 mm/min under the test standard ISO 2063-93. Mean tenacity and breaking extension are averaged from 50 observations for each yarn sample.

The properties of the yarns spun using 100% CT, 100% CS, and 50% CS/50%CT blends are given in Table 2. The experimental results show yarn tenacity increases with rising cotton fiber content. The pure cotton yarns show the highest tenacity and elasticity (elongation at break), and minimum irregularity (CV) values as compared with other yarns. Owing to the low strength and cohesion of the CS fiber, the pure CS yarn has the lowest tenacity and highest elongation irregularity (CV). As CS and CT fibers are blended, except for the tenacity irregularity (CV), the tenacity and elongation of the blended yarn increases greatly and the hairiness decreases.

Blend ratio CS/CT (%)	Tenacity (cN/tex)	Tenacity CV (%)	Elongation at break (%)	Elongation CV(%)	Hairiness index (H)
100/0	8.48	8.8	4.97	21.3	7.42
50/50	16.73	9	5.44	9	5.1
0/100	22.56	6.2	6.43	4	5.51

Table 2. Properties of (pure /blended) chitosan (CS)/cotton (CT) yarns in experimental conditions

Results and discussion

In this section, simulations were conducted to create a rotating flow in the spinning triangle, and to compute the dynamics of CS–CT fiber at different positions. Again, yarn structure and quality with experimental and numerical results were also discussed. For all the following computer-studied cases, the parameters of the CS–CT fiber are the same as our spinning experiment. The fiber length is 38 mm, and it is placed initially in an inclined plane between two cylinders (the roller nip), which has an angle of 45° from the horizontal plane (Figure 3). The trailing end of the fiber is out of the front roller nip and its lead-end is still inside. Along the z-axis, the fibers at the four different initial position ($z = 0$, 5, 7, 12 mm) are computed. It is noted that the cylinder length is 28 mm and only the fibers at one side of the cylinder center are simulated. The initial velocity of the bead that constitutes the fiber is equal to that of the fluid at the location of the bead centroid.

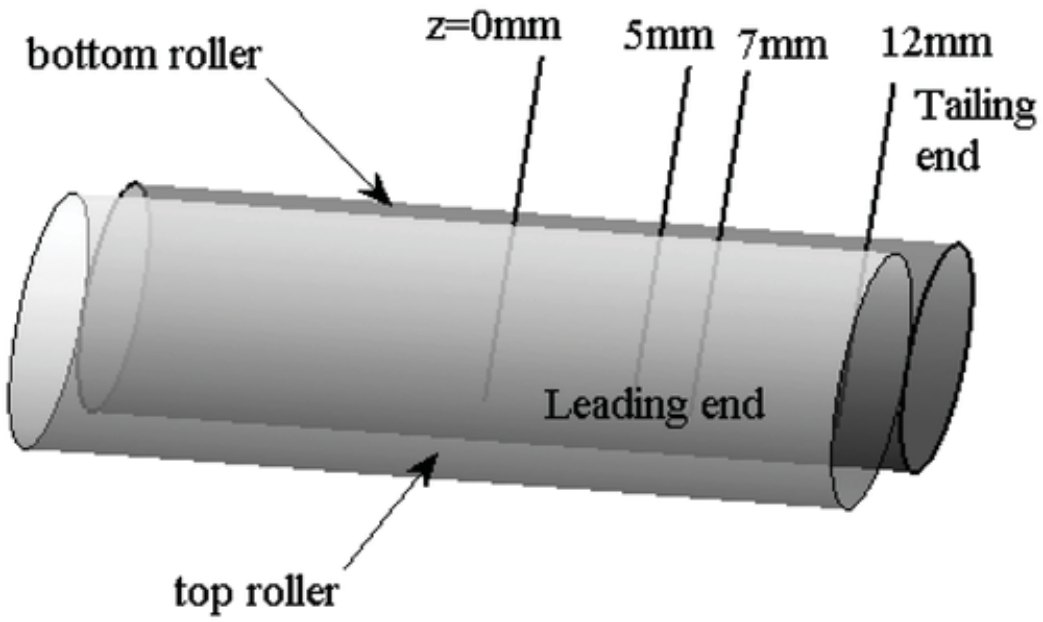

Figure 3. The initial positions of the computed fibers.

Dynamics of the CS–CT fiber

As shown in Figure 4, owing to the two cylinders rotating in the opposite direction, the velocity is greatest near the circular cylinders, and the stream-wise directions of the fluid around two cylinders are opposites. It is noted that the fluid is asymmetrical, especially in the roller nip (the inclined plane between two cylinders), due to different rotational velocities and diameters of the two rollers and their inclined position. Therefore, the fiber strands will form an asymmetric spinning triangle under the action of the asymmetric flow field. Simulation results well supported the spinning test and theory.[18] The fluid motion along the cylinder axis (*z*-axis) in the roller nip is similar to the magnetic induction line around the cylinder center. The vortex can be observed in the front upper of the top roller, and its size increases and the strength decreases gradually along the *z*-axis (from the cylinder center to its end).

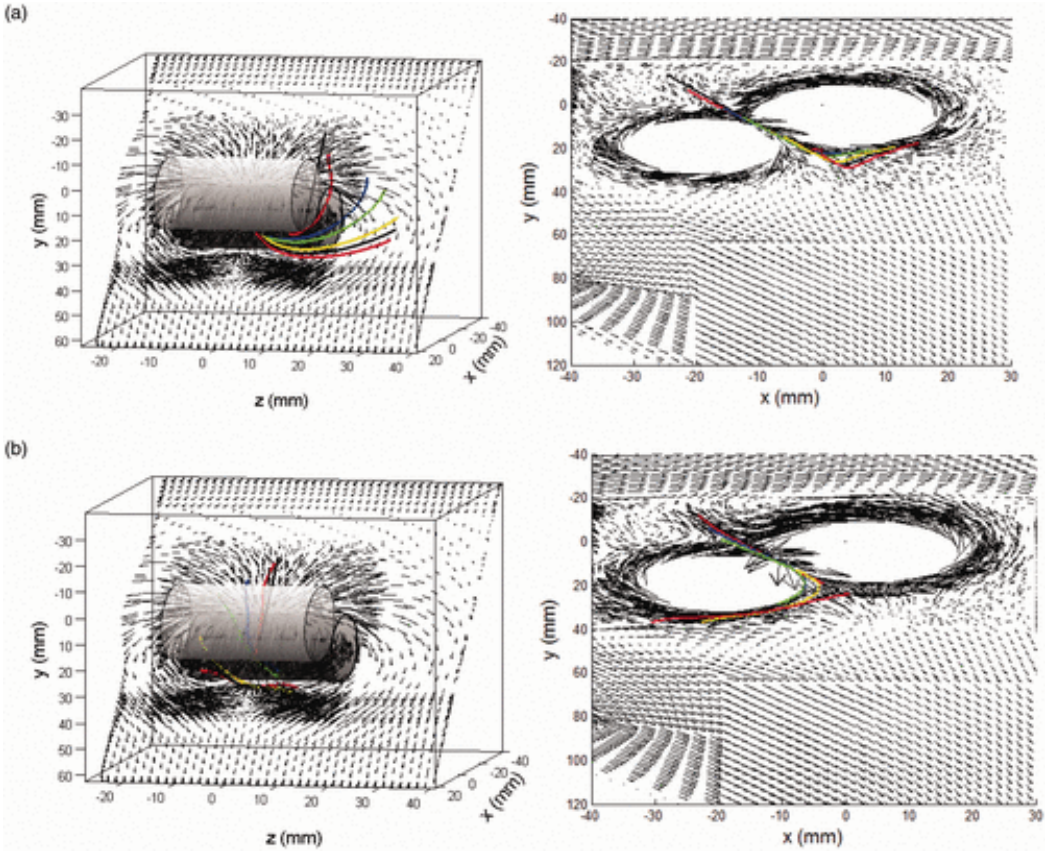

Figure 4. Fluid velocity vector and evolutions of CS fiber configurations on 3D and the *x*–*y* plane with different initial positions: (a) $z = 12$ mm; (b) $z = 0$ mm. The thick color lines indicate the fiber shapes at different times. The short black lines with arrows indicate the fluid velocity vectors.

It is seen in Figure 4a that due to the centrifugal force, as the CS fiber ($z = 12$ mm) lies at the edge of the cylinders, where the positions of the two end-planes of the cylinders are at $z = \pm 14$ mm, its tail-end part is off the roller nip, i.e., out of the cylinders, and its leading portion moves around the top roller (upper cylinder). Therefore, the fibers near the ends of the cylinder will shift out of the roller's nip. Corresponding to spinning theory and experience,[5,18] yarn hairiness or fly will be produced as the head and tail of the border fiber cannot be involved in the gauze. Similarly, the tail-end of the center CS fiber ($z = 0$ mm) also deflects gradually from the cylinder center due to the *z*-direction asymmetric fluid of the rotating flow (Figure 4b). However, the fiber is bound into the roller nip and its head-end moves toward the *z*-axis center and the bottom roller to form the spinning triangle. Note also that the fiber will straighten gradually in the triangle zone. This coincides with the formation principle of the triangle zone,[5,18] that the fiber assembly contains no twist in this zone.

As shown in Figure 4, the fibers with springy and snake-like configurations[7,9,19]simultaneously move along the stream-wise direction and rotate in a spiral orbit. This is because the rotating flow is helical. The trajectories of two end beads of the fibers in Figure 5 also show this, where all particle trajectories show helical shapes with stream-wise direction, especially, the tail-end of the fiber for all cases. For the fibers near the cylinder center, which is less than half the length corresponding to the cylinder center ($z = 0$ and 5 mm), their tail-ends in the negative stream-wise (y-axis) direction first move toward the opposite direction of their positions along the z-axis, i.e., the negative z-axis, and then toward the cylinder center as they reach the positive y direction (Figure 5a). Also, with the z-axis, the head-ends of the fibers near the center ($z = 0$ and 5 mm) move first in the opposite direction, and then they both go toward the cylinder center (Figure 5b). The simulation results, i.e., fiber trajectories, show the fibers in inner and outer layers can migrate and interweave with each other to increase the interfiber friction and form a triangle zone. This is in good agreement with the theory of the spinning triangle.[5,18] It is clear that the deflection of the tail-end of the fiber at $z = 5$ mm is larger than that of the fiber at $z = 0$ mm (Figure 5a). In addition, the tail-end of the fiber at $z = 5$ mm almost moving to the cylinder edge may lead to form tail-end hairiness.

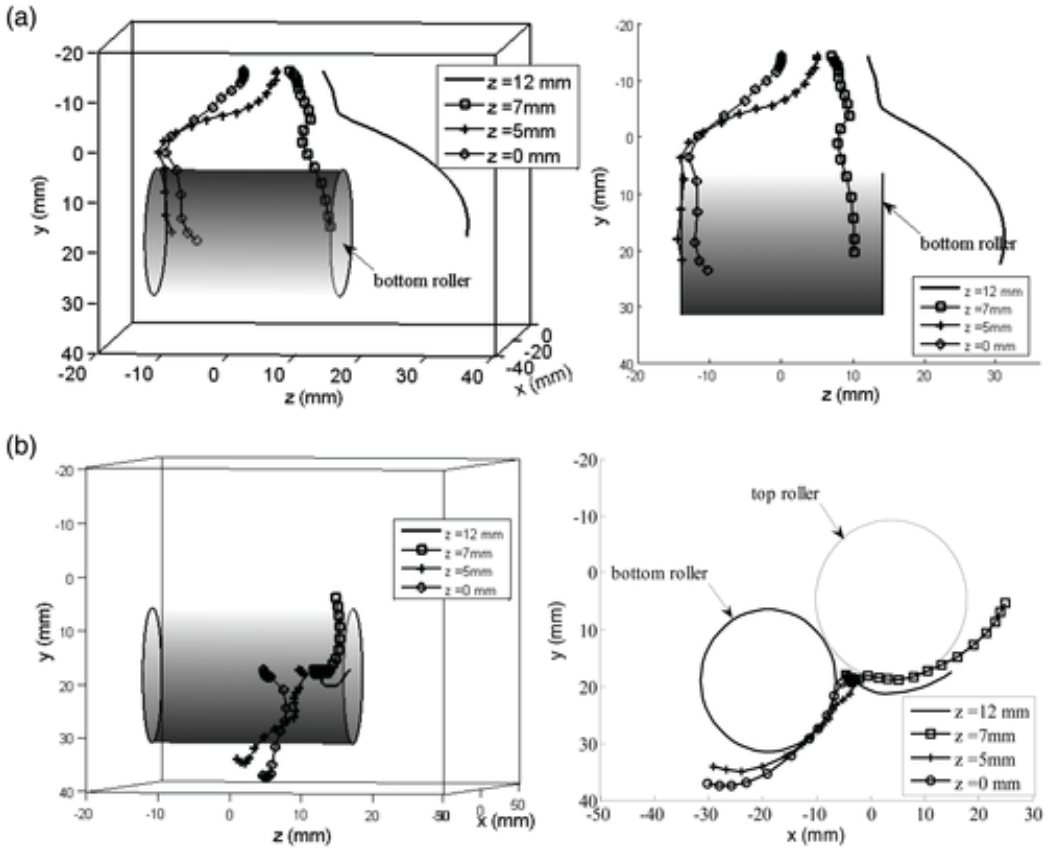

Figure 5. The trajectories of end beads of CS fibers with different initial position: (a) tail-end bead; (b) lead-end bead projection on the *xy* plane.

On the contrary, from Figure 5, the tail- and head-ends of the fibers ($z = 7$ and 12 mm) in the middle and edge of the cylinders shift along the positive z- and x-axes, respectively, due to stronger z directional fluid and the vortex in the front upper of the upper cylinder (see also the fluid field in Figure 4). Also, their lead-end will cover the surface of the top cylinder. Different from the edge fiber, the tail-end of the middle fiber ($z = 7$ mm) does not leave the cylinders; its head-end, however, moves around the top cylinder. Therefore, for the middle fiber, its tail-end will insert into the yarn in the triangle zone and the head-end is free, which will form heading hairiness and lead to unevenness.[5,18]

The spinning experiment shows that CS–CT fiber blending can improve yarn strength and unevenness (Table 2). To demonstrate this point from the fiber dynamics, Figure 6 shows the trajectories of end beads of CS and CT fibers with different initial positions. It can be observed from the figure that there is no obvious difference

between the (head- and tail-end) trajectories of CS and CT fibers as they lie in the middle of the half axis of the cylinders ($z = 7$ mm). It needs to be noted that the cotton fiber near the cylinder end also leaves the roller's nip as the CS fiber, which is not shown in the figure. For all fibers near the cylinder center ($z = 0$ and 5 mm), along z-axis, their tail-ends first move in the opposite direction of the axis, then toward the cylinder center. Again, they are bound into the cylinder's nip and, except the cotton fiber at $z = 5$ mm, they cover the surface of the bottom cylinder. Consequently, the triangle zone is formed. It is clear that for the cotton fibers near the cylinder center ($z = 0$ and 5 mm), the z-direction deflections of their tail-end are much smaller than those of CS fibers due to lower rigidity of CT fibers; thus, the pure cotton yarn can form a narrower and longer triangle compared to the pure CS yarn. Also, the pure CS yarn will form a wide triangle zone to decrease the fiber–fiber cohesion force, as a result, a lower yarn strength. According to the principle of ring spinning,[5] the long and narrow triangle zone implies a long weak point and causes more end breakages; however, the small triangle width can make that the edge fibers are better bound in the yarn, which gives smoother (less hairy) and stronger yarns. The spinning experiment also supports this; the pure cotton yarn has the greatest breaking extension (%) and strength and least unevenness and hairiness (see also Table 2). In addition, the simulation results show that CS fibers will migrate outwards in CS–CT blended yarn due to a greater z-direction offset of CS fibers. The spinning experiments of Lam and colleagues[4] support this, in which Hamilton migration indices of CS fibers are positive (i.e., outward migration) for all CS–CT blended yarn. Compared with pure CS and pure CT, CS–CT blended yarn has increased strength due to the inward migration of CT fibers, and improved antibacterial properties due to the outward migration of CS fibers.

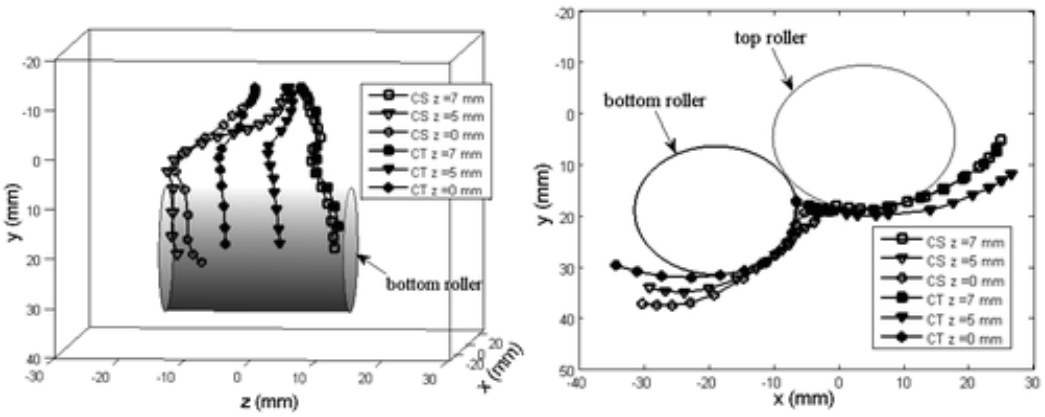

Figure 6. The trajectories of end beads of CS and CT fibers with different initial positions: left, tail-end bead; right, lead-end bead projection on the *x*–*y* plane.

Mechanical energy of the CS–CT fibers

The fibers sustain their motion and deformation by exchanging energy with the surrounding fluid. The elastic potential energy E_p is generated by the stretching/compression (E_s), bending (E_b), and twisting (E_t). It has three components ($E_p = E_s + E_b + E_t$), defined by Eq. (9).[10]

$$E_s = \int_0^{l_f} \frac{1}{2\pi r^2 E}(\mathbf{F}^s)^2 ds E_b = \int_0^{l_f} \frac{1}{2EI_b}(M_b)^2 ds E_t = \int_0^{l_f} \frac{1}{2GI_t}(M_t)^2 ds \tag{9}$$

where M_b and M_t are bending and torsional moments, respectively.

Note that the twisting potential energy, which is not shown in Figure 7, may be ignored because it is at least one order of magnitude lower than the bending energy. This further demonstrates that the fiber assembly contains no twist in the spinning triangle zone.[5] As shown in Figure 7a, for all cases, the stretching energy of CS fibers remains constant with time. The bending energy is the largest at $z = 0$ mm. However, it is the smallest at $z = 5$ mm because it has the largest stretching energy. The change of the bending energy at $z = 7$ mm is largest. Hence, the fiber at $z = 7$ mm can entangle

more fibers and increase hairiness because it moves toward the top roller. This also coincides with the spinning experiments (see also Table 2).

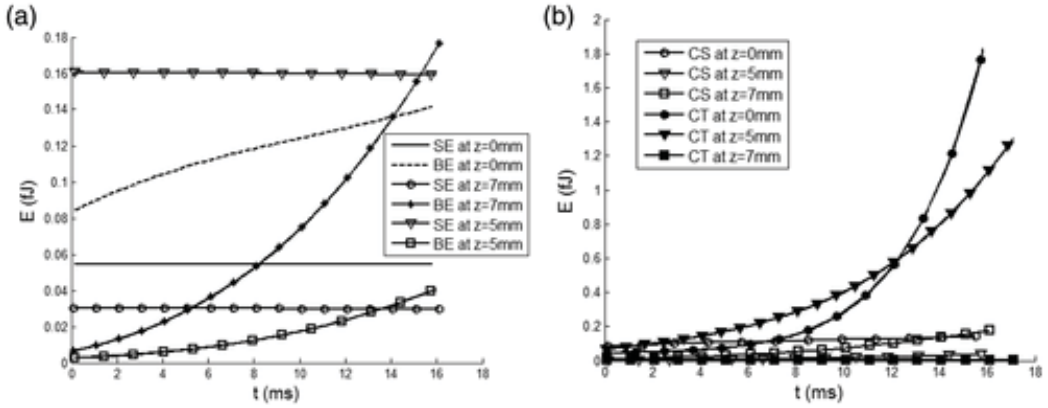

Figure 7. (a) Deformation energy of CS fiber at different positions; (b) bending potential energy of CS–CT fibers at different positions.

It is clear that the bending energy of cotton fibers is much larger than that of chitosan fibers, except for fibers at $z = 7$ mm (Figure 7b). Therefore, the cotton fiber near the cylinder center ($z = 0$ and 5 mm) can entangle more fibers to produce strength (see also Table 2). For the fiber at the middle of the half axis of the cylinders ($z = 7$ mm), the cotton has less bending energy. As chitosan and cotton fibers are blended, they combine to improve the yarn's properties (see also Table 2).

Conclusions

The extend bead–rod fiber model proposed by Guo and Xu[11,12] was applied to simulate CS–CT dynamics in 3D rotating airflow around two counter-rotating cylinders. The effects of different initial positions of CS–CT fibers on yarn properties were also discussed. The predictions of yarn properties correspond with the experimental and theory results.

For the most cases, the fibers near the cylinder end-face can leave the cylinder's nip and move around the top cylinder, thus form fly waste. The stretching energy remains constant with time, and the bending energy is the largest at $z = 0$ mm. Compared to chitosan fiber, the tail-ends of the cotton fibers have a much smaller negative direction deflection along the z-axis, and thus form a narrower triangle zone and

stronger yarns. The bending energy of cotton fiber is much greater than that of chitosan fiber.

Declaration of conflicting interests

The author(s) declared no potential conflicts of interest with respect to the research, authorship, and/or publication of this article.

Funding

The author(s) disclosed receipt of the following financial support for the research, authorship, and/or publication of this article: This research was supported by RGC Funding PolyU 154031/14H.

References

1. Liu XF, Guan YL, Yang DZ, et al. Antibacterial action of chitosan and carboxy methylated chitosan. *J Appl Polym Sci* 2001; 79: 1324–1335.
2. Eagle WYG. The effect of chitosan and its derivatives on the dyeability of silk. PhD Thesis, Hong Kong Polytechnic University, 2003.
3. Lim SH, Synthesis of a fiber-reactive chitosan derivative and its application to cotton fabric as an antimicrobial finish and a dyeing-improving agent. PhD Dissertation, North Carolina State University, USA, 2002.
4. Lam NYK, Zhang M, Guo HF, et al. Effect of fiber length and blending method on the tensile properties of ring spun chitosan–cotton blend yarns. *Text Res J* 2017; 87(2): 244–257.
5. Lawrence CA. *Advances in yarn spinning technology.* Cambridge: Woodhead Publishing Limited, 2010.
6. Yamamoto S and Matsuoka T. A method for dynamic simulation of rigid and flexible fibers in a flow field. *J Chem Phys* 1993; 98(1): 644–650.
7. Ross RF and Klingenberg DJ. Dynamic simulation of flexible fibers composed of linked rigid bodies. *J Chem Phys* 1997; 106(7): 2949–2960.
8. Dong S, Feng X, Salcudean M, et al. Concentration of pulp fibers in 3D turbulent channel flow. *J Multiphase Flow* 2003; 29: 1–21.
9. Schmid CF, Switzer LH and Klingenberg DJ. Simulations of fibre flocculation: effects of fibre proper- ties and interfibre friction. *J Rheol* 2000; 4: 781–809.
10. Gere JM and Timoshenko SP. *Mechanics of materials,* 2nd ed. London: Van Nostrand, Reinhold, 1987.
11. Guo HF and Xu BG. A novel method for dynamic simu- lation of flexible fibers in a 3D swirling flow. *Int J Nonlinear Sci* Numer Simul 2009; 10(11–12): 1473–1479.
12. Guo HF and Xu BG. A 3D numerical model for a flex- ible fiber motion in compressible swirling airflow. *CMES: Comput Model Eng Sci* 2010; 61(3): 201–222.
13. Klein W. *A practical guide to ring spinning, manual of textile technology*, Vol. 4. Manchester: The Textile Institute, 1987.
14. Batina JT. Unsteady Euler airfoil solutions using unstruc- tured dynamic meshes. *AIAA J* 1990; 28: 1381–1388.
15. Weatherill NP. Delaunay triangulation in computational fluid dynamics. Comp *Mathematics Appl* 1992; 24(5–6): 129–150.
16. Grant G and Tabakoff W. Erosion prediction in turbo- machinery resulting from environmental solid particles. *J Aircraft* 1975; 12(5): 471–478.

17. Doi M and Chen D. Simulation of aggregating colloids in shear flow. *J Chem Phys* 1989; 90: 5271–5279.
18. Hua T, Tao XM, Cheng KPS, et al. Effects of geometry of ring spinning triangle on yarn torque Part I: analysis of fiber tension distribution. *Textil Res J* 2007; 77: 853–863.
19. Forgacs OL and Mason SG. Particle motion in sheared suspension: X. Orbits of flexible threadlike particles. *J Colloid Sci* 1959; 14: 473–491.